References

[1]Syberg, J. and Koncsek, J. L. "Transonic and Supersonic Test of the SST Prototype Air Intake," FAA-SS-72-50, April 1972, Federal Aviation Administration, Washington, D. C.

[2]Koncsek, J. L. and Syberg, J., "Transonic and Supersonic Test of a Mach 2.65 Mixed-Compression Axisymmetric Intake," CR 1977, March 1972, NASA.

[3]Smeltzer, D. B. and Sorensen, N. E., "Analytic and Experimental Performance of Two Isentropic Mixed Compression Axisymmetric Inlets at Mach Numbers 0.8 to 2.65," TN D-7320, June 1973, NASA.

[4]Tjonneland, E., "The Design, Development and Testing of a Supersonic Transport Inlet System," Paper 18 presented at the NATO/AGARD 38th Meeting of Propulsion and Energetics Panel, Sandefjord, Norway, Sept. 1971.

[5]Sorensen, N. E., Smeltzer, D. B., and Cubbison, R. W., "Study of a Family of Supersonic Inlet Systems," *Journal of Aircraft*, Vol. 6, No. 3, May–June 1969, pp. 184–188.

[6]Whitlow, J. B., "Comparative Performance of Several SST Configurations Powered by Noise Limited Turbojet Engines," TM X-68178, Dec. 1972, NASA.

MAY 1974 J. AIRCRAFT VOL. 11, NO. 5

Arbitrary Pressure Gradient Integral Technique for Predicting Boundary Layer and Thermal Parameters

Richard J. Flaherty*
United Aircraft Research Laboratories, East Hartford, Conn.

A new nonequilibrium eddy viscosity model, based on an equilibrium eddy viscosity correlation and a turbulent energy balance, is used within an integral procedure to describe transport properties in turbulent boundary layers. In the analysis, velocity and temperature profiles are represented by conventional power laws with variable power law exponents which are determined from correlations of mass entrainment associated with both the momentum and thermal boundary layers. Stanton number is determined as a function of the Reynolds stress near the wall (but outside the influence of the laminar sublayer) and the shapes and relative sizes of the velocity and thermal boundary layers.

Nomenclature

C_f = wall friction coefficient, $\tau_w/(\frac{1}{2}\rho_e u_e^2)$
C_f' = peak Reynolds stress coefficient near the wall, $\rho_w\overline{u'v'}/(\frac{1}{2}\rho_e u_e^2)$
C_p = specific heat at constant pressure
H = δ^*/θ
H_i = $1 + 2n$
H_m = $1 + 2m$
k = thermal conductivity
M = Mach number
m = temperature profile exponent, $(T_t - T_w)/(T_{te} - T_w) = (y/\delta_h)^m$
n = velocity profile exponent, $u/u_e = (y/\delta)^n$
n_w = $rC_f'/0.14 + [(rC_f'/0.14)^2 + (rC_f'/0.14)]^{1/2}$
n^* = eddy viscosity parameter
P_r = laminar Prandtl number, $\mu C_p/k$
P_{rt} = turbulent Prandtl number (assumed to be 0.9)
P_{t_t} = total pressure at edge of boundary layer
$\bar{R}_h$ = weighted resistance, thermal
$\bar{R}_u$ = weighted resistance, momentum
r = $1 + [(T_{te}/T_e)^{1/2} - 1]\, e^{-0.02/\mathrm{In}1/3.1}$
S_T = Stanton number
s = surface distance
T = temperature
t = time
u = velocity
u' = turbulent velocity component in the flow direction
v' = turbulent velocity component normal to the wall
W = velocity boundary layer mass thickness, $\int_0^\delta \rho u/\rho_e u_e\, dy$
W_h = thermal boundary layer mass thickness, $\int_0^{\delta_h} \rho u/\rho_e u_e\, dy$
y = distance normal to wall
y^+ = $(\frac{1}{2}\rho_w\rho_e^2 C_f')^{1/2} y/\mu_w$
γ = ratio of specific heats
δ = velocity boundary-layer height
δ^* = boundary-layer displacement thickness
δ_h = thermal boundary-layer height
ϵ = kinematic eddy viscosity
Θ = momentum deficity thickness, $\int_0^\delta \rho u/\rho_e u_e(1 - u/u_e)\, dy$
μ = viscosity
τ = shear
ϕ = thermal energy deficity thickness, $\int^{\delta_h} \rho u/\rho_e u_e(1 - T_t/T_{te})\, dy$

Subscripts

aw = adiabatic wall
e = edge of the boundary layer
t = total (stagnation) conditions
w = wall
p = heat transfer reference point in the boundary layer ($200\, y^+$)
ref = Eckerts reference temperature

Presented as Paper 73-700 at the AIAA 8th Fluid and Plasma Dynamics Conference, Palm Springs, Calif., July 16–18, 1973; submitted August 20, 1973; revision received February 28, 1974.

Index category: Boundary Layers and Convective Heat Transfer—Turbulent.

*Senior Research Engineer.

Introduction

A PHYSICAL description of an integral method for predicting laminar and turbulent boundary-layer growth and heat transfer is presented. In this method the von Kármán boundary-layer momentum integral equation is numerically integrated in the streamwise direction using auxiliary equations to compute the form factor and skin friction. Velocity and temperature profile shapes needed for the analysis are determined from mass entrainment models which utilize a new nonequilibrium eddy viscosity formulation for turbulent flow situations.

The present entrainment method, developed to fulfill a need for a simple-to-use, yet accurate and fast boundary-layer predictive scheme, has been applied successfully to

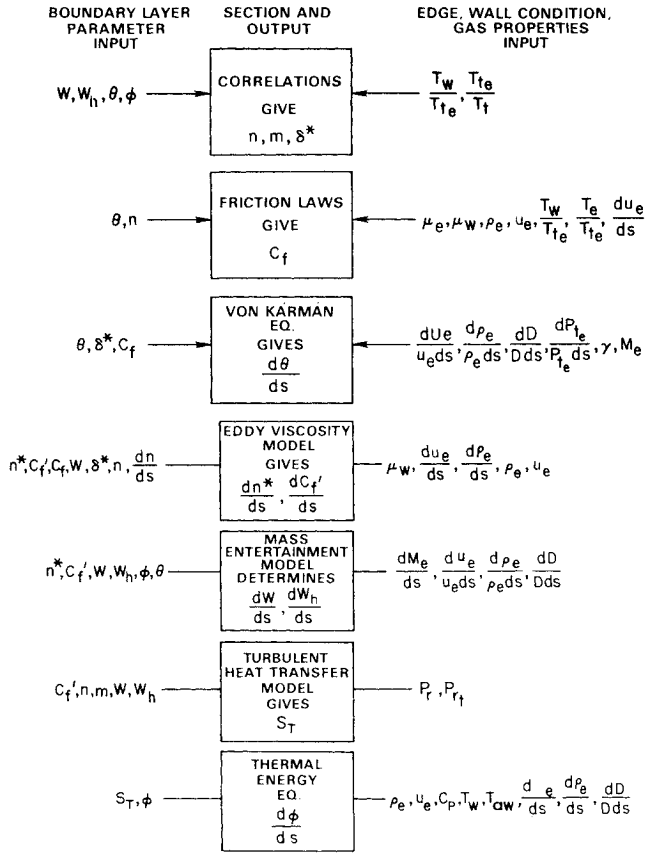

Fig. 1 Input and output of the different sections of the procedure.

many diverse problems in rocket engines, ramjets, laser devices, inlets, and diffusers. A major advantage of an entrainment approach is that it can account for the entrainment of mass into a thermal boundary layer that is much smaller than the velocity boundary layer. This permits the computation of the heat transfer with arbitrary wall temperature distributions by the method of superposition.

The basic parameters that are desired from a boundary-layer computational procedure are the momentum thickness Θ; the displacement thickness δ^*; the Stanton number S_T; and the skin friction coefficient C_f, or parameters that are functions of one of these variables such as wall shear stress and heat transfer rate. The present integral method for estimating such boundary-layer and heat transfer parameters in arbitrary pressure gradients is developed from a number of separate models. This paper describes the over-all approach, and gives a physical description of the more important models employed in this method. In addition, comparisons are made with available data to indicate the versatility and accuracy of the analytical method.

Description of Method

Analytical Flow Chart

The present turbulent procedure determines six primary boundary-layer parameters. These are 1) the mass (weight flow) in the velocity boundary layer W, 2) the momentum defect Θ, 3) the mass in the thermal boundary layer W_h, 4) the thermal defect ϕ, 5) the peak eddy viscosity parameter, n^*, and 6) the peak turbulent shear coefficient near the wall C'_f. All other boundary-layer parameters such as wall skin friction coefficient C_f, displacement thickness δ^*, Stanton number S_T, and the velocity and thermal profile parameters n and m are determined from one or more of these six parameters along with edge conditions, wall conditions, and gas properties. For laminar flow, n^* and C'_f do not exist.

An analytical flow chart of the basic sections (major models, correlations, and primary equations) used in the present procedure and the output of that section is shown on Fig. 1. The boundary parameter inputs into each section are shown on the left side of the figure and the corresponding edge, wall, and gas property inputs into that section are shown on the right side of the figure. The parameters shown inside the boxes are those determined from that section of the analysis.

In order to perform an integration of the primary boundary-layer parameters in the streamwise direction s, the derivative of each of the six primary parameters is needed. The von Kármán equation determines $d\Theta/ds$; the thermal energy equation, using the Stanton number determined from the turbulent heat transfer model, determines $d\phi/ds$; the mass entrainment expressions determines both dW/ds and dW_h/ds; and the nonequilibrium eddy viscosity model determines dn^*/ds and dC'_f/ds

Correlations

In the present analysis, both velocity and total temperature profiles are represented by conventional power laws.

$$\frac{u}{u_e} = \left(\frac{y}{\delta}\right)^n \tag{1}$$

$$\frac{T_t - T_w}{T_{t_e} - T_w} = \left(\frac{y}{\delta h}\right)^m \tag{2}$$

The variable power law exponents are determined from correlations involving the masses contained in the velocity and thermal boundary layers, the momentum and energy defects, and the ratio of the total to static temperatures.

The boundary-layer correlations section is shown in Fig. 1 as determining n and m (profile shape parameters—velocity and thermal, respectively) as a function ϕ, Θ, W, W_h. However, the correlations can also be used to give W, and W_h if ϕ, Θ, m, and n are given. The ratio of the wall temperature to stagnation temperature $T_w/T_{t(e)}$ and the freestream total to static temperature $T_{t(e)}/T_e$ are needed, of course, for either analysis. The correlating expressions are developed.[1] As an example, the expression used for determining n, the velocity power law exponent, is

$$\frac{W + \phi}{\theta} = \frac{1 + 2n}{n}\left(1 + \frac{(T_{t_e}/T_e - 1)^{1/2}}{3.1} e^{-\frac{0.02}{\ln l}}\right) \tag{3}$$

Additional correlations are used for computing the ratio of the displacement thickness to the momentum thickness, and the thermal power law exponent m.

Skin Friction Laws

Wall skin friction for turbulent boundary layers is determined using the incompressible approach of Escudier, Nicoll, and Spalding,[2] adjusted for compressibility and wall temperature effects by an approximation to the method of Spalding and Chi.[3] Development of the turbulent skin friction relationships is presented.[1] The empirical laminar skin friction law used reduces to the conventional flat plate laminar law when the shape factor assumes a flat plate value.[1] Both laminar and turbulent skin friction relationships employed are based on a shape factor and a momentum defect Reynolds number. In situations when significant flow acceleration occurs, such functional relationships often under predict the wall shear stress. Therefore, in the present procedure, an acceleration wall shear coefficient, designated C_{fa}, is used for C_f

wherever it exceeds the value that the turbulent (or laminar) friction law gives. The acceleration skin friction, C_{fa}, is based on two-dimensional stagnation flow on a cylinder.[1]

von Kármán Equation

The change in the momentum thickness in the streamwise direction s is determined from an expanded form of the von Kármán integral boundary layer equation:

$$\frac{d\theta}{ds} = \frac{C_f}{2} - \theta\left(\frac{d\rho_e}{\rho_e ds} + \frac{du_e}{u_e ds}(2 + H) + \frac{dD}{Dds}\right) + \frac{\delta^* dP_{te}}{\gamma M_e^2 P_{te} ds} \quad (4)$$

The last term in Eq. (4) is added to account for any total pressure loss in the freestream.[1] Determinations of the shape factor H and the skin friction coefficient C_f were discussed. The other terms in Eq. (4) are determined from the flow conditions at the edge of the boundary layer and the system geometry. The parameter D is a flow divergence term; in axisymmetric flow D could be either the radius or diameter.

Eddy Viscosity Model

The eddy viscosity is used to determine the rate of mass entrainment into the velocity boundary layer. Since it also determines the rate of mass entrainment into the thermal boundary layer, it is the tie between the velocity and thermal boundary layers.

The eddy viscosity model developed can be employed in integral form for both equilibrium and nonequilibrium turbulent boundary layers. Experimental eddy viscosity data for equilibrium boundary layers was correlated to establish the basic model. Modifications were then introduced to extend the model to nonequilibrium cases.

Equilibrium eddy viscosity correlation

The kinematic eddy viscosity model used is based on a correlation of the kinematic eddy viscosity for equilibrium boundary layers

$$\frac{\epsilon}{u_e n\delta\left(1 + 0.06\frac{\gamma - 1}{2} M_e^2\right)} = f\left(\frac{y}{\delta}\right)$$

demonstrated in Fig. 2 using experimental data.[4,5] Analytical curves[6] also are shown. Maise and McDonald[6] present a correlation of flat plate adiabatic wall velocity profile data for the Mach number range from 0 to 5.0. Eddy viscosity profiles consistent with the development of these velocity profiles were determined[6] and are shown here based on the present eddy viscosity correlating parameter.

A slight Mach number dependence is included in the present eddy viscosity model, but the most significant portion of this correlating parameter is $n\delta$ where n is the power law exponent and δ is the boundary-layer height.

Eddy viscosity profile approximations

In the present integral procedure it is necessary to be able to integrate analytically the reciprocal of the total viscosity (molecular plus eddy viscosity) multiplied by a weighting function across the boundary layer from the wall to any y value in the boundary layer to determine the effective resistance from the wall to that location. This requires a mathematically simple representation of the eddy viscosity profile. The following model was selected; the eddy viscosity is represented by the two straight lines as shown in Fig. 2.

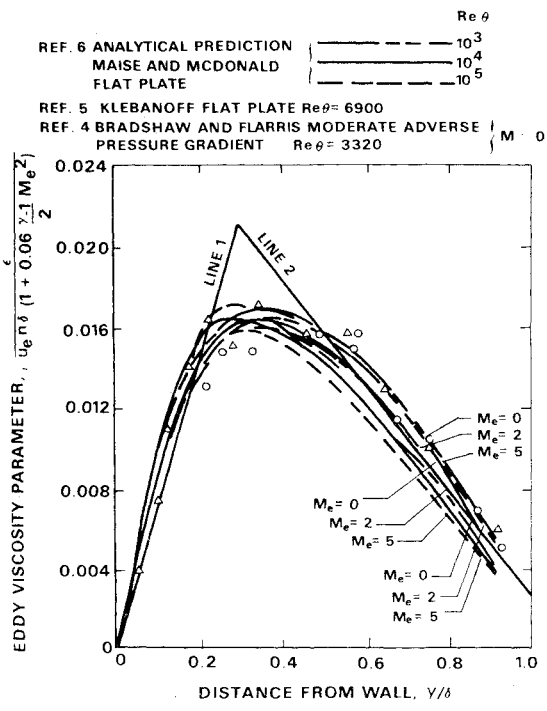

Fig. 2 Kinematic eddy viscosity correlation.

The maximum value of eddy viscosity and the peak turbulent shear near the wall is used for construction of the eddy viscosity distribution in the boundary layer. The peak turbulent shear determines the slope of the linear eddy viscosity increase away from the wall and the maximum eddy viscosity determines the value where this linear increase stops.

Nonequilibrium eddy viscosity

The eddy viscosity correlations shown in Fig. 2 are for equilibrium boundary layers which do not change shape or shear distribution with distance. For nonequilibrium boundary layers these eddy viscosity levels can be incorrect by as much as a factor of 3.[7]

The maximum eddy viscosity parameter is defined as

$$n^* = n\frac{\epsilon_{max}(\text{actual})}{\epsilon_{max}(\text{equilibrium})}$$

It is determined by following the production and dissipation of turbulent energy along a "streamline" at the approximate transverse location in the boundary layer where the maximum is expected.

The local production of turbulent energy is equal to the product of the shear stress and the local velocity gradient, and turbulent energy is equal to the shear stress multiplied by an empirical constant. The local dissipation of the turbulent energy into heat is proportional to the 3/2 power of the turbulent energy. For an equilibrium boundary layer at any axial location the production and dissipation are equal (except for the net production required as the boundary layer grows.) Thus, the unknown constant of proportionality for the decay of turbulent energy into heat is determined from the equilibrium conditions, and gives the decay constant as a function of boundary-layer parameters.

Changes in the freestream velocity are based on experimental data[7] from incompressible flow which shows that for sudden velocity changes the shear along a turbulent "streamline" does not immediately follow the change in velocity but initially remains constant. This fact permits the inclusion into the model of changes in the eddy viscosity caused by changes in freestream velocity. That is, the

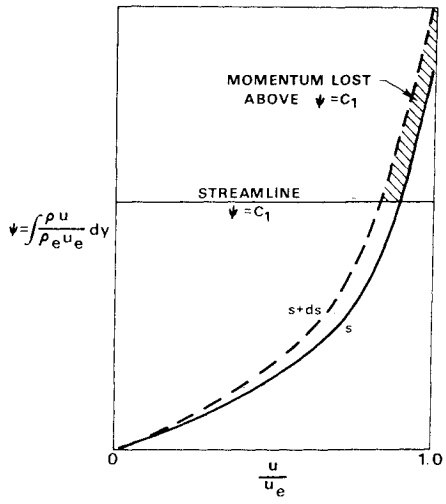

Fig. 3 Flat plate entrainment.

shear stress immediately after the sudden velocity change with the new velocity gradient normal to the wall, must equal the turbulent shear stress before the velocity change. Thus, the new value of eddy viscosity can be determined, since the new normal velocity gradient is known from the new velocity power law exponent.

The effect of three other parameters on the maximum eddy viscosity also is included in the model in an approximate matter. These include the effect of mass entrainment, freestream density changes, and nonequilibrium transfer of turbulent energy normal to the wall.

There is no effect of mass entrainment on the equilibrium value of the eddy viscosity. Therefore, it is assumed that the turbulent energy of mass entrained is that associated with the equilibrium eddy viscosity value, and that any change in the eddy viscosity due to mass entrainment can be mass weighted with the new mass having the equilibrium value.

The effect of freestream density changes on the eddy viscosity is based on the conservation of angular momentum. If a vortex is compressed, its angular momentum stays constant but its velocity increases. This increase in kinetic energy is obtained from the work of compression. Thus, the turbulent energy must increase when the density increases and decrease when the density decreases. However, all the turbulent energy in boundary layers is not in the form of vortices (whirlpool-type eddies), so the turbulent energy change must be some fraction of the change which would occur if it were all in the form of vortices. The fraction of total turbulent energy assumed to be in the form of vortices was one-fourth.

There is an assumed nonequilibrium transfer of turbulent energy in the boundary layer normal to the wall when deviations in the shape of the eddy viscosity profile from that of the equilibrium profile occur. These deviations result in changes in the maximum eddy viscosity parameter.

The expression for dn^*/ds is[1]

$$\frac{dn^*}{ds} = \frac{n_w}{\delta}\left(1 - \left(\frac{n^*}{n}\right)^{1/2}\right) + \frac{0.5n^*}{\rho_e}\frac{d\rho_e}{ds} - \frac{n^*dn}{nds} - \frac{2n^*du_e}{u_e ds} + n^*\frac{(n-n^*)}{w}\frac{dW}{ds} + 0.07\left(\frac{n_w^2 - n^{*2}}{\delta}\right) \quad (5)$$

The maximum turbulent shear stress (Reynolds stress, $\overline{\rho v'u'}$) is normally near the wall but outside of the region laminar influence. In strong adverse pressure gradients it can occur closer to the center of the boundary layer than to the wall. For moderate pressure gradients the peak Reynolds stress essentially is equal to the wall shear and the slope of the eddy viscosity with distance from the wall is a function of the skin friction coefficient. The relationship derived[1] shows the slope as nearly proportional to the square root of the skin friction coefficient for moderate pressure gradients.

In highly accelerating flows the maximum Reynolds stress can be significantly less than the wall shear stress. The pressure gradient gives the high wall shear stress from purely laminar considerations and also gives a shear stress gradient across the laminar sublayer. The assumption is made that for a sudden change in the freestream velocity the Reynolds stress near the wall must remain constant (the same as further from the wall). It is assumed that the recovery of this stress to the value of the wall shear stress is proportional to the product of: 1) the difference between the skin friction coefficient and the Reynolds stress coefficient, 2) the ratio of the maximum eddy viscosity in the boundary layer to the viscosity at the wall, and 3) the flow distance divided by a scale length related to laminar sublayer thickness. Since turbulent heat transfer is a function of $\overline{\rho u'v'}$ near the wall rather than the wall shear stress, Stanton number data obtained at relatively low Reynolds numbers under different acceleration conditions was used to determine the constant of proportionality. The expression for (dC'_f/ds) is[1]

$$\frac{dc_f'}{ds} = (c_f - c_f')\frac{\rho_e u_e n^* \delta}{640,000\mu_w y_{10}} - \frac{2}{u_e}\frac{du_e}{ds}c_f' \quad (6)$$

Where y_{10} is the y value where $y^+ = 10$ and

$$c_f' \equiv \left(\frac{\overline{\rho u'v'}}{\frac{1}{2}\rho_e u_e^2}\right)_{\max}$$

The kinematic eddy viscosity near the wall (line 1 on Fig. 2) is

$$\epsilon = 0.07\, u_e n_w (1 + 0.06\frac{\gamma - 1}{2}M_e^2)y \quad (7)$$

where

$$n_w = \frac{rc_f'}{0.14} + \left[\left(\frac{rc_f'}{0.14}\right)^2 + \frac{rc_f'}{0.14}\right]^{1/2} \quad (8)$$

Since $rC'_f/0.14$ is small n_w is close in value to $(rC'_f/0.14)^{1/2}$. For equilibrium flat plate flow both n^* and n_w equal n.

Mass Entrainment Expressions

The mass entrainment expression is derived from flat plate equilibrium flow considerations. It is based on the following physical facts: 1) the change in momentum defect above any "streamline" in the flat plate boundary layer must equal the integral of the shear along that "streamline," and 2) the equilibrium boundary layer does not alter its shape (see Fig. 3). These considerations result in the establishment of an entrainment rate which is related to transport phenomena via the eddy viscosity correlation. For nonequilibrium flat plate flows a correction is introduced using the ratio of the resistances of the boundary layer in question and the flat plate equilibrium boundary layer with the same characteristic eddy viscosity parameter. In accelerating flows, mass is detrained from the velocity boundary layer. For example, the amount of mass between the wall and some reference velocity (i.e., $u/u_e = 0.995$) decreases in a strong acceleration. To account for this, an empirical mass detrainment expression is employed which is a function of the Mach number and its variation, and the ratio of thermal to momentum defects.

For flat plate equilibrium flows[1]

$$(dW/ds) = 0.07n^* \quad (9)$$

Heat Transfer Model

The heat transfer into (or out of) a boundary layer from the wall can be determined if the temperature difference

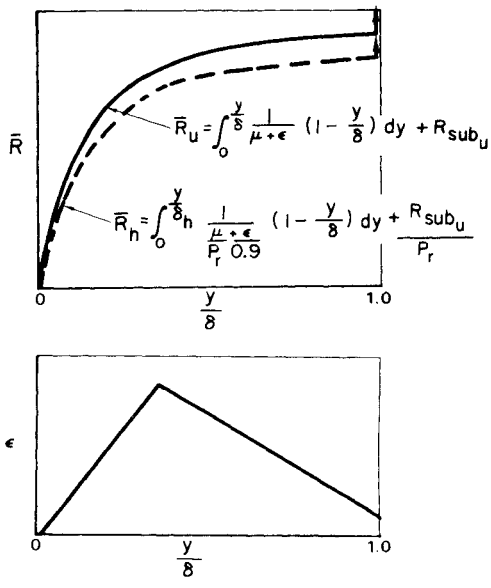

Fig. 4 Conversion of eddy viscosity profile to weighted resistances.

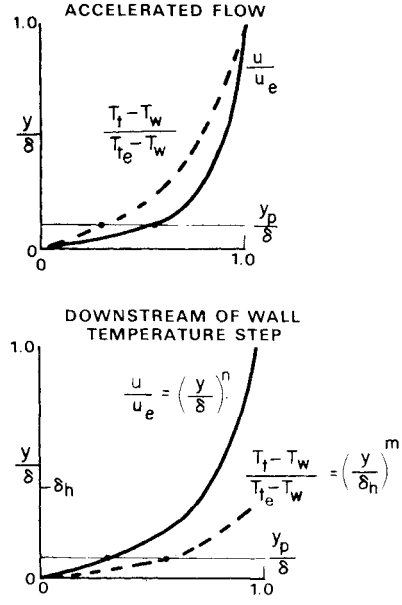

Fig. 5 Physical description of heat transfer model.

between a point in the boundary layer near the wall and the wall itself is known along with the thermal resistance between the point and wall. The point must be near to the wall compared to the boundary-layer height since all the heat must pass through the region adjacent to wall but is deposited in (or withdrawn from) the flow in the rest of the boundary layer. With the present eddy viscosity model, the resistances (thermal and momentum) from the wall to any point in the boundary layer can be estimated. The momentum resistance per unit length is equal to the reciprocal of total viscosity. The integral of the unit resistance from the wall to a point in the boundary layer gives the resistance to the point.

The resistance across the boundary layer must be weighted. Take for example a hot wall boundary layer. In this case, all the heat transfer must pass through the region near the wall but the heat is deposited in the fluid as a temperature change as the heat passes through the boundary layer. Also consider flat plate boundary layers in which the shear decreases with distance from the wall because the shear force is absorbed in the fluid as a momentum defect. An electrical analogy to the heat transfer and flat plate shear stress would be a main line carrying current that is bled off by users along the line. A weighted or effective resistance for the main line with its users could be determined by integrating along the main line the product of the main line resistance and the local current in the main line divided by the current entering the main line at the power plant. A similar weighted resistance will be determined for the boundary layer using the relative shear stress across the flat plate boundary layer. The shear stress relationship across a flat plate boundary layer is shown.[6] A rough approximation to this relationship used herein is a linear decrease in shear stress over δ. Figure 4 shows the typical graph of the weighted resistances as a function of y/δ. The equations given in Fig. 4 show how the laminar and turbulent Prandtl numbers enter into the thermal resistance. (The turbulent Prandtl number is assumed to be 0.9). It is assumed that μ (the molecular viscosity) and ρ are equal to their freestream values; i.e., $\mu = \mu_e$ and $\rho = \rho_e$. Also a laminar sublayer resistance R_s is added since there is a small region immediately next to the wall where turbulence cannot exist and the eddy viscosity is zero. Although this sublayer region is physically small (assumed to reach to $y^+ = 10$ in the present procedure) its resistance is significant since it is pure laminar and it must be incorporated into the resistance model.

Because of the manner in which the resistances are determined in the present procedure (i.e., $\rho = \rho_e$ and $\mu = \mu_e$), the ratio of the thermal to momentum resistances is considered more accurate for compressible flow than either of the resistances. Thus, the Stanton number is obtained from the Reynolds stress coefficient near the wall C'_f, by comparing the relative velocity potential with the relative temperature potential from the point near the wall. The difference between the momentum and thermal resistances from this point to the wall are due to the laminar and turbulent Prandtl numbers. Therefore, the ratio of these resistances is included to account for the Prandtl number effects. Nonequal relative velocity and thermal potentials are illustrated on Fig. 5. The top case is for accelerated flow with the thermal and velocity boundary layers of the same height. In the bottom case, the thermal boundary layer starts for downstream from the origin of the velocity boundary layer. If both cases had the same C'_f, the lower case would have the higher heat transfer. The reference point y_p is illustrated on Fig. 5. Ideally, one would like to take y_p as the outer edge of the laminar sublayer. However, the power law assumptions used herein are not valid that close to the wall in the boundary layer. The value of y, where $y^+ = 200$, appears to give good results when used for y_p. (An upper limit of 0.15δ is put on y_p.) With the assumption of thermal and velocity power law profiles for conditions where $\delta_h > y_p$

$$S_T = \frac{c_f'}{2}\left(\frac{y_p}{\delta}\right)^{(m-n)}\left(\frac{\delta}{\delta_h}\right)^m \frac{\bar{R}_{pu}}{\bar{R}_{ph}} \tag{10}$$

It will be assumed that the ratio of velocity boundary-layer thickness to thermal boundary-layer thickness,

$$\delta/\delta_h \approx \left(\frac{W}{W_h}\right)^{\frac{1}{n+1}}$$

For incompressible flow with $W_h < W$ this expression for δ/δ_h can be obtained as an equality by direct integration. When the thermal boundary is below the reference point y_p (e.g., when the velocity boundary layer has started far upstream of the point where the thermal boundary layer originates), the weighted thermal resistance to the edge of the thermal boundary layer $R_{\delta(h)}$ will be ratioed to the weighted momentum resistance to the reference point.

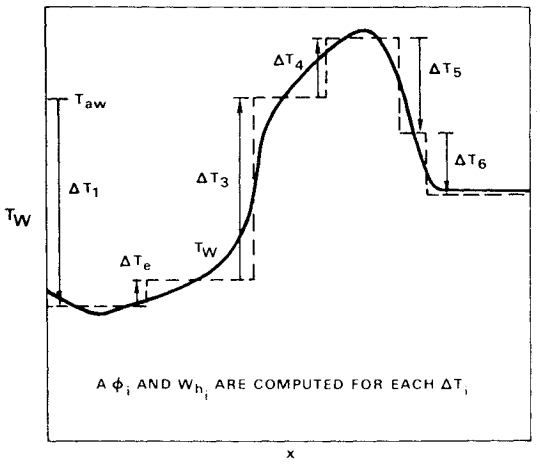

Fig. 6 Superposition.

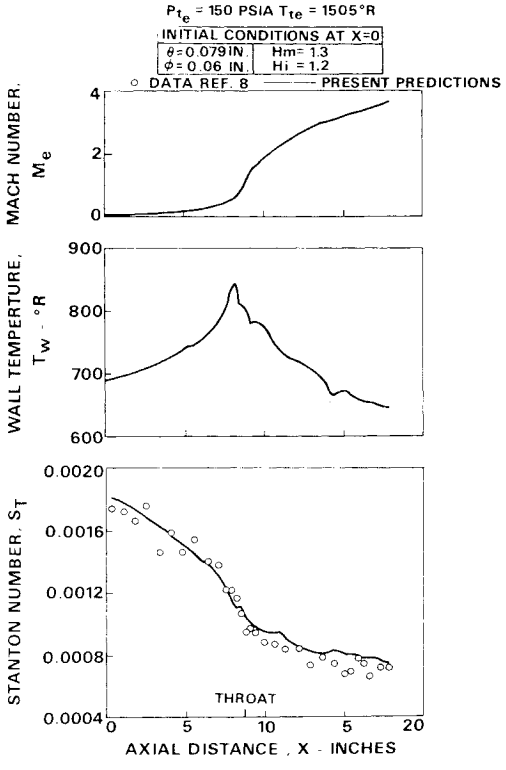

Fig. 7 Cooled nozzle heat transfer.

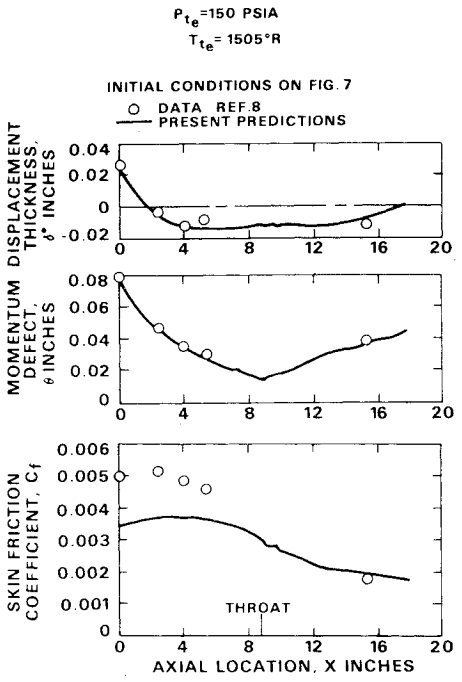

Fig. 8 Boundary-layer parameters for cooled nozzle.

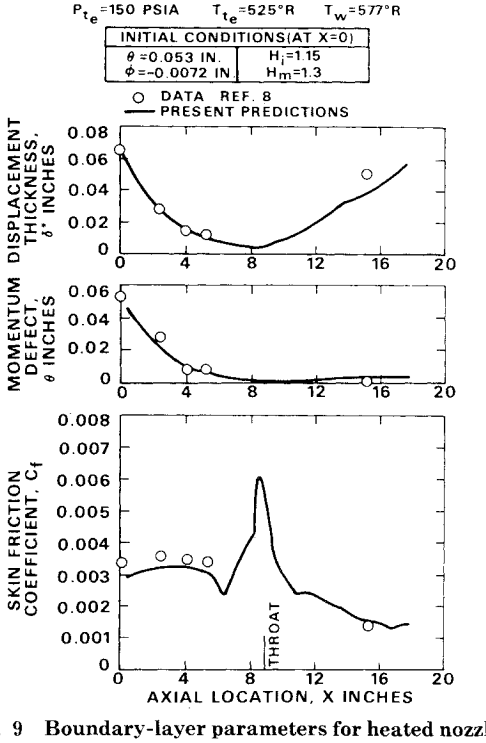

Fig. 9 Boundary-layer parameters for heated nozzle.

Thus for $\delta_h < y_p$

$$S_T = \frac{c_f'}{2}\left(\frac{y_p}{\delta}\right)^{-n}\frac{\bar{R}_{pu}}{\bar{R}_{\delta h}} \tag{11}$$

With the Stanton number known for Eqs. (7) or (8), the change in ϕ with respect to s is given by the (thermal) energy equation

$$\frac{d\phi}{ds} = S_T\left(\frac{T_{aw} - T_w}{T_{t_e}}\right) - \phi\left(\frac{1}{\rho_e u_e}\frac{d(\rho_e u_e)}{ds} + \frac{dD}{Dds}\right) \tag{12}$$

The ratio of resistances across the thermal and velocity boundary layers determines the ratio of the mass entrainment rate in these layers. For example, a thermal boundary layer with half the effective resistance of the velocity boundary layer will entrain mass at twice the rate of the velocity boundary layer.

For situations in which the wall temperature varies in the streamwise direction, a superposition of solutions of the integral thermal mass entrainment model is employed. The wall temperature streamwise distribution is approximated by a series of steps as illustrated in Fig. 6, with a separate thermal boundary layer initiated at each temperature step. To account for the effect of heat transfer on the density in the boundary layer the superposition solutions are run simultaneously. Therefore, the incremental heat transfer from each of the separate solutions is summed up at each streamwise location for use in computing the boundary parameters at the following computational location.

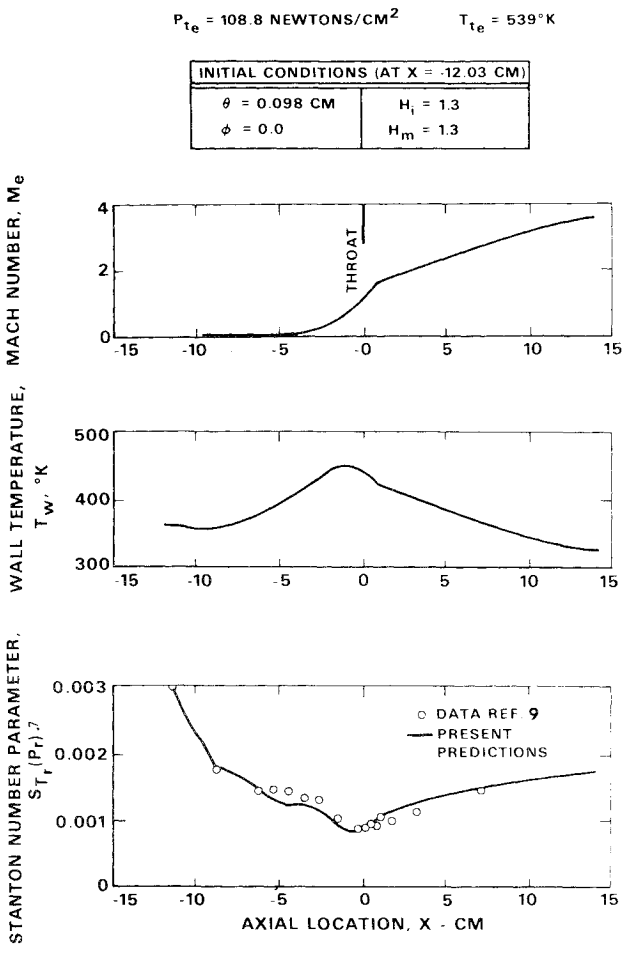

Fig. 10 Heat transfer in a cooled nozzle with uncooled inlet (low pressure).

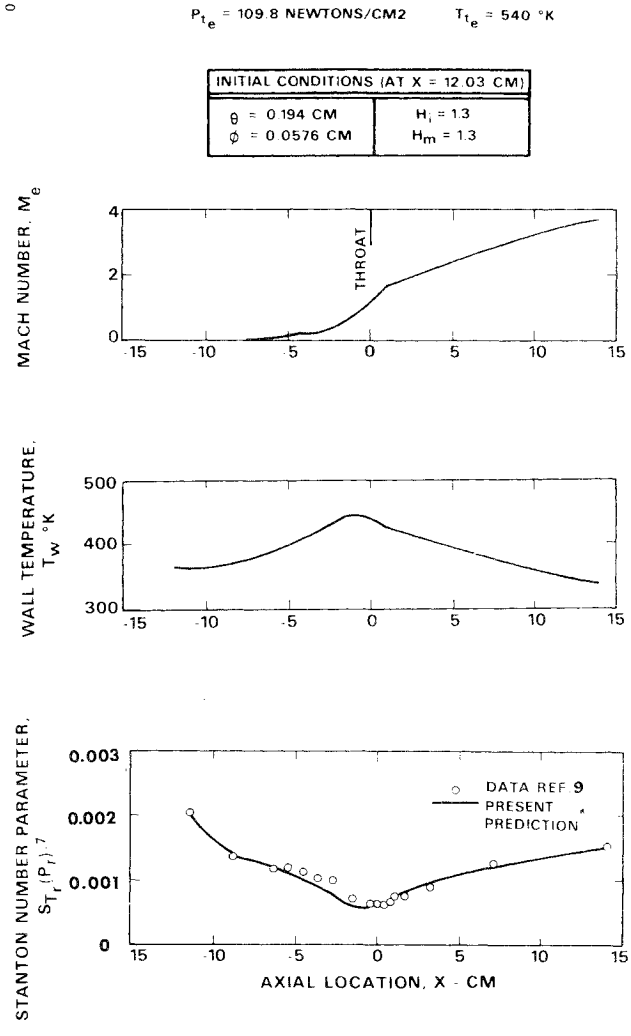

Fig. 11 Heat transfer in a cooled nozzle with cooled inlet (low pressure).

The use of superposition is a very powerful tool. For example, it can handle the case of a hot wall suddenly stepped back to the adiabatic wall temperature. It is obvious in this case that the hot boundary layer will transfer heat back into the wall even though the wall is at the adiabatic wall temperature. This heat transfer can be predicted by the superposition procedure.

Comparisons with Data

Turbulent Boundary-Layer Cases Involving Heat Transfer

Tests including heat transfer measurements in a cooled axisymmetric nozzle were reported.[8] During these tests, boundary-layer profiles surveys were made at several axial stations. From these profiles, calculations were made to determine the boundary-layer displacement, thermal defects, momentum defects, and skin friction. The axial Mach number and wall temperature distributions for the first case to be discussed is shown in Fig. 7. Note that distances are measured from Survey Station 1.[8] In this case, gas properties (such as Prandtl number, gas constant, viscosity, ratio of specific heats, etc.) are that of ideal air.

The measured Stanton number data for this first case compared to the prediction of the present method are also shown on Fig. 7. The predicted values are in close agreement with the measured values and the predicted curve has the same shape as a curve fared through the data would have. The initial conditions for Θ and ϕ were obtained from the data given.[8] The initial velocity and thermal shape parameters H_i and H_m, respectively, were estimated from the velocity and thermal profiles provided.[8]

The measured boundary displacement δ^*, momentum defect Θ, and estimated values of C_f obtained from profile measurements are compared to the integral method results in Fig. 8. In general, the agreement is good except for the friction coefficient in the $x = 0$ to 6 in. region. In this region the boundary-layer profile surveys did not extend down into the laminar sublayer as did the survey near the end of the nozzle. Thus the original C_f estimates may be in error. The use of these original C_f estimates with the present boundary-layer theory to compute corresponding Stanton numbers would increase the predicted value about 30% in the region $x = 0$ to 6 in.

Some boundary-layer profile surveys were also made[8] for the case where the nozzle wall was heated to 10%, above the total temperature of the gas flowing through the nozzle. The comparison between the measured and predicted boundary-layer parameters for these conditions are shown in Fig. 9. There is no Stanton number data for this case. The high skin friction prediction in the throat region is due to the momentum defect Reynolds number becoming very small and is considered artificial.

For cases such as the later one (hot wall) the accuracy of skin friction laws that use a Reynolds number based on Θ where Θ can go to zero (or even negative with a high enough wall temperature) is quite questionable. For the type of skin friction laws that a Θ determines, taking the maximum velocity in the boundary layer as an edge velocity and integrating from this point to the wall to obtain a Θ for use in these C_f equations would probably be more appropriate.

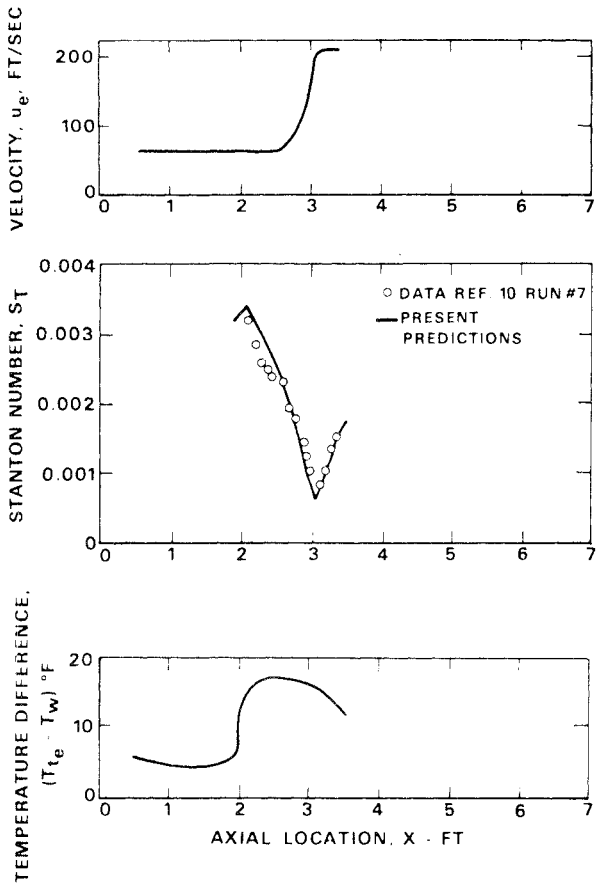

Fig. 12 Heat transfer with early high acceleration.

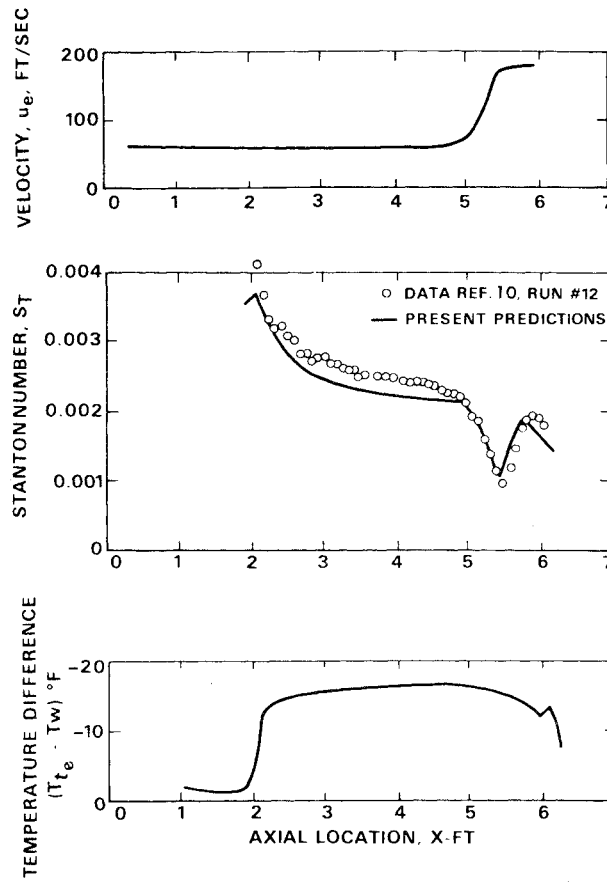

Fig. 13 Heat transfer with late high acceleration.

Heat transfer measurements in a cooled axisymmetrical nozzle were reported.[9] An inlet upstream of the nozzle could be either uncooled or cooled resulting in either a large or negligible thermal boundary layer entering the nozzle. Figures 10 and 11 compare the heat transfer measurements[9] (both with and without a cooled inlet) with the present integral method predictions. Data were presented in the form $S_{T(r)}(P_r)^{0.7}$ where $S_{T(r)} = S_T T_{\text{ref}}/T_e$ and T_{ref} is Eckerts reference temperature ($T_{\text{ref}} = 0.22\ T_{aw} + 0.5\ T_w + 0.22\ T_e$).[9] For these two figures, the present prediction are presented in the same form to permit comparison. The present method predicts both the shape and values of the $S_{T(r)}(P_r)^{0.7}$ variation with axial location x quite well for both the cooled and uncooled inlet cases. The initial values of Θ and ϕ were obtained.[9] The initial values of H_i and H_m were assumed to be 1.3. The gas is air.

A series of two-dimensional flow heat transfer tests at relatively low subsonic speeds using air with steps in the wall temperature and in some cases flow acceleration are reported.[10] For all cases[10] compared herein, the total pressure was near atmospheric and total temperature near 100°F. All of these cases (comparisons with Moretti and Kays[10] data) were initiated as a laminar start with no momentum or thermal defect at $x = 0$. Transition Reynolds numbers of 300 or 350 based on momentum defect were assumed to make the transition occur at the approximate location of the boundary trip used.[10] The velocity distributions shown for any of the data[10] were obtained from very small figures[10] and in some cases a discrepancy between velocity and the quoted values of Reynolds based on x could not be resolved.

The predicted and measured values for cases involving high acceleration are compared on Figs. 12 and 13. In general, the agreement between prediction and measurement is good. The difference between prediction and data in the constant velocity regions could be due to the Reynolds number discrepancy previously discussed. The constant for the inner layer history (Reynolds stress near the wall) was obtained empirically by determining the value which gave best agreement with the data level for these and other cases. However, the prediction made with this constant also gives the right slope and the proper lag for the drop off and recovery of the Stanton number. (The minimum Stanton number occurs downstream of the maximum acceleration parameter, $(\mu/\rho_e u_e^2)\ (du_e/ds)$.) The inner layer history model is used in all predictions, including the previous nozzle predictions, although it has little effect in those cases.

The measured and predicted Stanton numbers for a case[10] which has mild acceleration with repeated steps in the wall temperature is shown in Fig. 14. The present integral method, although not always predicting the levels exactly, does follow the shape of Stanton number distribution with location quite well.

Calculation Through a Normal Shock

The boundary-layer parameters (but not C_f) through a normal shock induced boundary-layer separation and reattachment were measured and reported.[11] The top curve in Fig. 15 shows the Mach number distribution used in computing this case. This distribution was obtained from the static pressure measurements[11] with the assumption of a constant total pressure. A correct Mach number distribution could be obtained if a total pressure loss distribution were known. Also shown on this figure are the measured values of Θ, H, the separation location, and the reattachment location. The predicted values of Θ, H. C_f obtained by the present integral method are indi-

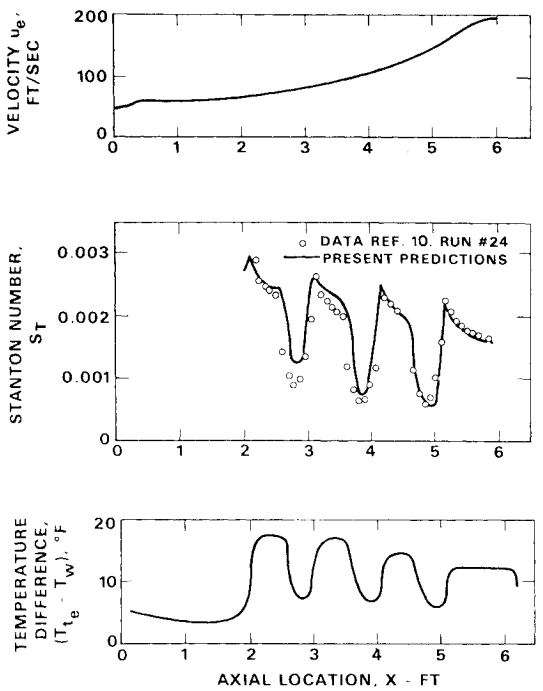

Fig. 14. Heat transfer with alternating wall temperature steps.

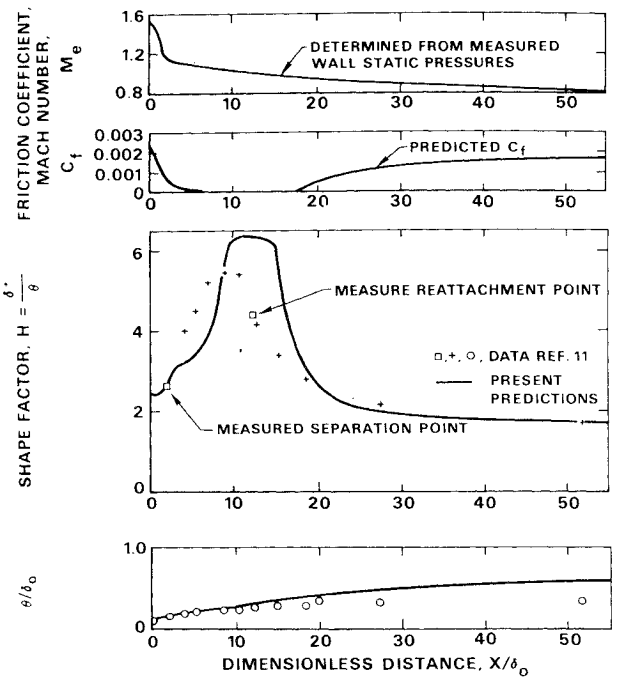

Fig. 15 Calculation through a strong adverse pressure gradient.

cated in Fig. 15. The predicted value of C_f should go to zero at separation and assume a positive value at reattachment. The present method predicts both the separation point and the reattachment point downstream of where they physically occur.

Conclusions

The present method for calculation of turbulent boundary layers is in agreement with data for predictions of boundary parameters and even heat transfer in cases of high acceleration. For extreme deceleration, leading to separation, the present method is in fair agreement with data. Because of the short computation time (about 10 sec per case on an 1108) and the proven ability to handle arbitrary pressure gradients, the method is considered a useful and practical engineering tool.

References

[1]Flaherty, R. J., "An Integral Procedure for Estimating Boundary Layer Parameters and Heat Transfer in Arbitrary Pressure Gradients," Rept. M110570-2, United Aircraft Research Labs., East Hartford, Conn. (to be published).

[2]Escudier, M. P., Nicoll, W. B., and Spalding, D. B., "An Explicit Drag Law for Uniform Density Turbulent Boundary Layer on Smooth Impermeable Walls, Tech. Note. TWF/TM/12, 1966, Department of Mechanical Engineering, Imperial College of Science and Technology, London, England.

[3]Spalding, D. B. and Chi, S. W., "The Drag of a Compressible Turbulent Boundary Layer on a Smooth Flat Plate With and Without Heat Transfer," *Journal of Fluid Mechanics*, Vol. 18, Jan. 1964, pp. 117.

[4]Bradshaw, P. and Ferriss, D. H., "The Response of a Retarded Equilibrium Turbulent Boundary Layer to a Sudden Removal of Pressure Gradient," Aero Rept. 1145, March 1965, National Physical Lab., England.

[5]Klebanoff, P. S., "Characteristics of Turbulence in a Boundary Layer with Zero Pressure Gradient," Rept. 1247, 1955, NACA.

[6]Maise, G. and McDonald, H., "Mixing Length and Kinematic Eddy Viscosity in a Compressible Boundary Layer," Rept. E211557-1, June 1966, United Aircraft Research Labs., East Hartford, Conn.

[7]Goldberg, P., "Upstream History and Apparent Stress in Turbulent Boundary Layers," Ph.D. theses, May 1966, Dept. of Mechanical Engineering, MIT, Cambridge, Mass.

[8]Back, L. H. and Cuffell, R. F., "Turbulent Boundary Layer Nozzle," *ASME Journal of Heat Transfer*, Vol. 93, Ser. C, No. 4, Nov. 1971, pp. 397–407.

[9]Boldman, D. R., Schmidt, J. F., and Eblers, R. C., "Prediction of Local and Integrated Heat Transfer in Nozzle Using an Integral Turbulent Boundary Layer Method, TN D-6595, March 1972, NASA.

[10]Moretti, P. M. and Kays, W. M., "Heat Transfer to a Turbulent Boundary Layer with Varying Free-Stream Velocity and Varying Surface Temperature—An Experimental Study," *Heat Mass Transfer*, Vol. 8, 1965, pp. 1187–1202.

[11]Seddon, J., "Flow Produced by Interaction of a Turbulent Boundary with a Normal Shock Wave of Sufficient Strength to Cause Separation," Tech Memo. Aero 667, 1960, Royal Aircraft Establishment, Farnborough, England.